Decentralized Civil Structural Control using Real-time Wireless Sensing and Embedded Computing

Yang Wang [a], R. Andrew Swartz [b], Jerome P. Lynch *[b], Kincho H. Law [a],
Kung-Chun Lu [c], Chin-Hsiung Loh [c]

[a] Dept. of Civil and Environmental Engineering, Stanford Univ., Stanford, CA 94305, USA
[b] Dept. of Civil and Environmental Engineering, Univ. of Michigan, Ann Arbor, MI 48109, USA
[c] Dept. of Civil Engineering, National Taiwan Univ., Taipei, Taiwan

* Correspondence Author:

Jerome P. Lynch
Assistant Professor
Department of Civil and Environmental Engineering
The University of Michigan
2380 G. G. Brown Building
Ann Arbor, MI 48109-2125 USA
Email: jerlynch@umich.edu

Abstract

Structural control technologies have attracted great interest from the earthquake engineering community over the last few decades as an effective method of reducing undesired structural responses. Traditional structural control systems employ large quantities of cables to connect structural sensors, actuators, and controllers into one integrated system. To reduce the high-costs associated with labor-intensive installations, wireless communication can serve as an alternative real-time communication link between the nodes of a control system. A prototype wireless structural sensing and control system has been physically implemented and its performance verified in large-scale shake table tests. This paper introduces the design of this prototype system and investigates the feasibility of employing decentralized and partially decentralized control strategies to mitigate the challenge of communication latencies associated with wireless sensor networks. Closed-loop feedback control algorithms are embedded within the wireless sensor prototypes allowing them to serve as controllers in the control system. To validate the embedment of control algorithms, a 3-story half-scale steel structure is employed with magnetorheological (MR) dampers installed on each floor. Both numerical simulation and experimental results show that decentralized control solutions can be very effective in attaining the optimal performance of the wireless control system.

Key words: structural control, wireless communication, embedded computing, decentralized control, velocity feedback control

1. Introduction

As an effective method of reducing the dynamic response of structures during earthquakes or typhoons, structural control technologies have attracted a great amount of interest from structural engineering researchers and practitioners over the past few decades (Soong and Spencer, 2002). About 50 buildings and towers were instrumented with various types of structural control systems from 1989 to 2003 (Chu *et al*., 2005), with evident reduction in structural dynamic responses being reported. Current structural control systems can be categorized into three major types: (a) passive control (e.g. base isolation), (b) active control (e.g. active mass dampers), and (c) semi-active control (e.g. semi-active variable dampers). Passive control has the advantage of power efficiency, while active control has the advantage of being adaptable to real-time excitations. As a hybrid between these two approaches to structural control (active and passive), semi-active control effectively combines the advantages of both systems. Examples of semi-active actuators include active variable stiffness (AVS) devices, semi-active hydraulic dampers (SHD), electrorheological (ER) dampers, and magnetorheological (MR) dampers. Another attractive feature of semi-active control systems is that they are inherently stable because their actuators do not apply mechanical energy directly to the structure.

In both semi-active and active control systems, sensors are employed in the structure to collect real-time structural response data during dynamic excitation (e.g. wind or earthquake). The response data is then fed into a single or multiple control decision modules (controllers) in order to determine control forces and apply commands to system actuators in real-time. According to these command signals, the structural actuators generate control forces intended to reduce unwanted structural vibrations. In traditional semi-active or active control systems, coaxial wires are normally used to provide communication links between sensors, actuators and controllers. For a typical low-rise building, the installation of a commercial wire-based data acquisition (DAQ) system can cost upwards of a few thousand dollars per sensing channel (Celebi, 2002). As the

size of the control system grows (defined by the nodal density and inter-nodal spatial distances), the additional cabling needed may result in increases in installation time and expense (Solomon *et al*., 2000). To capitalize on future low-cost semi-active devices that are densely installed in a structure, wireless communication technology can be adopted to eradicate the coaxial cables associated with traditional control systems. Although wireless communication has been widely explored for use in structural monitoring applications (Straser and Kiremidjian, 1998; Lynch and Loh, 2006a; Wang *et al*., 2007), application to real-time feedback control in structural engineering has been scarce (Lynch and Tilbury, 2005). Outside of structural engineering, a few examples of wireless control systems have been reported (Eker *et al*., 2001; Ploplys *et al*., 2004).

When replacing wired communication channels with wireless ones for feedback structural control, difficulties include coordination of the wireless nodes in a collaborative control network, degradation of real-time performance, and higher probability of data loss during transmission. The degradation of the control system's real-time characteristics is a common problem faced by distributed network control systems, regardless of using wired or wireless communication (Lian *et al*., 2002). Among the different solutions proposed for this problem, one possible remedy is the adoption of decentralized control strategies (Sandell *et al*., 1978; Lynch and Law, 2002). In a decentralized control system, the sensing and control network is divided into multiple subsystems. Controllers are assigned to each subsystem and require only subsystem sensor data to make control decisions. Therefore, reduced use of the communication channel is offered by a decentralized control architecture, which results in higher control sampling rates. Furthermore, decentralized control requires relatively shorter communication ranges, enabling more reliable wireless data transmissions. The drawback of decentralized control is that decentralized system architectures may only achieve sub-optimal control performance compared with centralized counterparts, because each subsystem only has its own state data from which it must calculate

control decisions. This work attempts to investigate the effectiveness of decentralized wireless control in civil structures.

This paper first introduces a prototype wireless structural sensing and control system developed by the authors (Wang *et al*., 2006). The system consists of multiple stand-alone wireless sensors that form an integrated network through a common wireless communication channel. Each wireless sensor can record response data from sensors, calculate control forces, communicate state data, and command actuators. In order to investigate the effects of communication latencies on centralized and decentralized wireless control strategies, centralized and decentralized output feedback control algorithms are implemented. The decentralized control method is developed by applying appropriate shape constraints to the gain matrix of a normal optimal output feedback control problem. Numerical simulations show that the higher sampling rates achievable by decentralized control may compensate for the disadvantage of incomplete sensor data from which control decisions are made. Large-scale shake table experiments are conducted on a 3-story steel frame structure installed with MR dampers to compare the performance of different decentralized and centralized control schemes.

2. A Prototype Real-time Wireless Sensing and Control System

To illustrate the architecture of the prototype wireless sensing and control system, Fig. 1 shows a 3-story structure controlled by three actuators. Wireless sensors and controllers are mounted on the structure for measuring structural response data and commanding actuators in real-time. Besides the wireless sensing and control units that are necessary for data collection and the operation of the actuators, a remote command server with a wireless transceiver is included in the system to initiate the operation of the control system and to log the flow of wireless data. To initiate the operation of the control system, the command server first broadcasts a start signal to all of the wireless sensing and control units. Once the start command is received, the wireless

units that are responsible for collecting sensor data start acquiring and broadcasting data at a preset time interval. Accordingly, the wireless units responsible for commanding the actuators receive the sensor data, calculate desired control forces, and apply control commands within the specified time interval allotted at each time step. The following describes in detail the design of the wireless sensing and control units. Specific attention is paid to the control signal generation and wireless communication modules of the wireless unit since both are integral to the performance of the global control system.

2.1 Hardware Design for the Wireless Sensing and Control Unit

The wireless unit is designed in such a way that the unit can serve as either a sensing unit (i.e. a unit that collects data from sensors and wirelessly transmits the data), a control unit (i.e. a unit that calculates control forces and commands actuators), or a unit for both sensing and control. This flexibility is supported by an integrated hardware design based upon a wireless sensing unit previously proposed for wireless structural monitoring by Wang *et al*. (2007). Three basic functional modules are included in the wireless sensing unit design: sensor signal digitizer, computational core, and wireless transceiver. The wireless control unit contains the same three modules as the wireless sensing unit, but also includes a supplementary control signal generation module designed to reside off-board of the basic wireless sensor. The architectural design of the wireless control unit is presented in Fig. 2(a). The architectural design of the wireless sensing unit can be obtained by simply omitting the control signal generation module. A simple two-layer printed circuit board (PCB) for the wireless sensing unit is designed and fabricated (Fig. 2b). As shown in Fig. 2(c), the PCB, wireless transceiver, and batteries are stored within an off-the-shelf weatherproof plastic container, which has the dimensions of 10.2cm by 6.5cm by 4.0cm.

The sensor signal digitization module of the wireless unit contains a 4-channel 16-bit Texas Instrument ADS8341 analog-to-digital (A/D) converter. This module converts the 0 to 5V analog

output of up to four sensors (to date, different types of transducers have been successfully interfaced including accelerometers, velocity meters, LVDTs and strain gages) into digital formats usable by the wireless sensor's computational core. The digitized sensor data is transferred to the computational core through a high-speed serial peripheral interface (SPI) port. The computational core consists of a low-power 8-bit Atmel ATmega128 microcontroller and an external 128kB static random access memory (SRAM) chip for data storage. For wireless communication among the sensing units, two types of wireless transceivers may be employed: 900MHz MaxStream 9XCite and 2.4GHz MaxStream 24XStream (MaxStream, 2005). Generally, the 9XCite is used in the U.S. and other countries where 900MHz is open to unlicensed usage while the 24XStream is used internationally on the 2.4GHz radio band. When a wireless unit is designated as a sensing unit, its wireless transceiver is primarily used to send sensor data out to the wireless network. In contrast, for a wireless control unit, its wireless transceiver receives sensor data from the network. After receiving the sensor data, the ATmega128 microcontroller embedded in the wireless control unit computes the desired control forces. Once the control force calculation is completed, the wireless control unit issues commands (voltage signals) to the actuator through the control signal generation module. All of the hardware components of the wireless sensing unit, not including the wireless transceiver, consume about 32mA when active and 80μA when in stand-by mode. The additional power consumption of the two wireless transceivers (9XCite and 24XStream) will be presented in section 2.3.

2.2 Control Signal Generation Module

A separate hardware module is designed to be connected with the wireless sensing unit, which permits the unit to generate analog voltage signals for commanding actuators. At the core of this control signal generation module is the single-channel 16-bit digital-to-analog (D/A) converter, the Analog Device AD5542. The AD5542 receives a 16-bit unsigned integer from the ATmega128 and converts the integer value to an analog voltage output spanning from -5 to 5V.

Additional support electronics are included in the control signal generation module to offer stable zero-order hold voltage outputs at high sampling rates (1 MHz maximum). The wide voltage output range (-5 to 5V) of the control signal generation module, particularly the negative output range, is one of the key features of the module's design. With the wireless sensing unit designed to operate on 5V, the Texas Instruments PT5022 switching regulator is integrated in the signal generation module to convert the 5V regulated power supply into a stable -5V reference. Another auxiliary component required for the AD5542 to generate a bipolar -5 to 5V output signal is a rail-to-rail input and output operational amplifier, for which the National Semiconductor LMC6484 operational amplifier is selected. The typical slew rate of the LMC6484 is about 1.3V/μs, which means that the output voltage can swing about 1.3V within 1μs. This output gradient is compatible with the microsecond-level settling time of the AD5542 D/A converter. When operational, the control signal generation module draws about 70mA from the 5V power supply provided by the wireless sensing unit.

As shown in Fig. 3(a), a separate double-layer printed circuit board (PCB) is designed to accommodate the D/A converter (AD5542) and its auxiliary electrical components. The control signal board is attached via two multi-line wires to the wireless sensor. To reduce circuit noise, two separate wires are used with one dedicated to analog signals and the other to digital signals. The analog signal cable transfers an accurate +5V reference voltage from the existing wireless sensing board to the signal generation module. The digital signal cable provides all of the connections required to accommodate the serial peripheral interface (SPI) between the ATmega128 microcontroller and the AD5542. To command an actuator, a third wire is needed to connect the output of the control signal generation module with the structural actuator. The control signal generation module connected to the wireless sensing unit is shown in Fig. 3(b).

2.3 Wireless Communication Module

A challenge associated with employing wireless sensors in a structural control system is the performance of the wireless communication channel. When the wireless sensors are used within a wireless structural monitoring system, robust send-acknowledgement communication protocols are used to ensure that no data is lost (Lynch *et al.*, 2006b). However, the real-time requirements of the control system do not permit sufficient time for the use of send-acknowledgement communication protocols that ensure channel reliability. Furthermore, stochastic delays in the channel are probable; these delays cannot be deterministically accounted for *a priori* in the control solution formulation (Seth *et al.*, 2004). For these reasons, an appropriate wireless transceiver that minimizes data loss without sacrificing communication speed must be judiciously selected for use in the wireless control system.

The wireless sensing unit is designed to be operable with two different wireless transceivers: 900MHz MaxStream 9XCite and 2.4GHz MaxStream 24XStream. Pin-to-pin compatibility between these two wireless transceivers makes it possible for them to share the same hardware connections in the wireless unit. Because of the different data rates, embedded software for using the two transceivers is slightly different. This dual-transceiver support offers the wireless sensing and control unit more flexibility in terms of not only use in different geographical areas, but also provides different data transfer rates, communication ranges, and power consumption characteristics. Table 1 summarizes the key performance parameters of the two wireless transceivers. As shown in the table, the data transfer rate of the 9XCite is twice that of the 24XStream, while the 24XStream provides a longer communication range but consumes more battery power. The peer-to-peer communication capability of the two wireless transceivers makes it possible for the wireless sensing and control units to communicate with each other, thus supporting flexible information flow among multiple wireless units. In this study, validation tests of the wireless sensing and control system are performed using a test structure at the National Center for Research on Earthquake Engineering (NCREE) in Taipei, Taiwan. Because of the

local frequency band requirements in Taiwan, the MaxStream 24XStream wireless transceiver operating on the 2.4GHz spectrum is employed for the experimental tests.

As previously discussed, one critical issue in applying wireless communication technology to real-time feedback structural control problems is the communication latency encountered when transmitting sensor data from the wireless sensing units to the wireless control units. The anticipated transmission time of the 24XStream radio for a single data packet is illustrated in Fig. 4. The transmission time consists of the communication latency ($T_{Latency}$) of the radios and the time to transfer data between the microcontroller and the radio using the universal asynchronous receiver and transmitter (UART) interface (T_{UART}). Assume that the data packet to be transmitted contains N bytes and the UART data rate is R_{UART} bps (bits per second), which is equivalent to R_{UART} /10 bytes per second, or R_{UART} /10000 bytes per millisecond. It should be noted that the UART transmits 10 bits for every one byte (8-bits) of sensor data due to start and stop bits. The communication latency in a single transmission of this data packet can be estimated as:

$$T_{SingleTransm} = T_{Latency} + \frac{10000N}{R_{UART}} \text{ (ms)} \quad (1)$$

In the prototype wireless sensing and control system, the setup parameters of the 24XStream transceiver are first tuned to minimize the transmission latency, $T_{Latency}$. Then experiments are conducted to measure the actual $T_{Latency}$, which turns out to be 15±0.5ms. The UART data rate of the 24XStream radio, R_{UART}, can be selected among seven different options, ranging from 1200 bps to 57600 bps. After considering the UART performance of the ATmega128 microcontroller operated at 8MHz, R_{UART} is selected as 38400 bps in the implementation. If a data packet sent from a sensing unit to a control unit contains 11 bytes, the total time delay for a single transmission is estimated to be:

$$T_{SingleTransm} = 15 + \frac{10000 \times 11}{38400} \approx 17.86 \,(\text{ms}) \qquad (2)$$

This single-transmission delay represents the communication constraint that needs to be considered when calculating the upper bound for the maximum sampling rate for the control system. Another deciding factor for the sampling rate is the number of wireless transmissions needed at each control sampling step. A few milliseconds of safety cushion time at each sampling step is a prudent addition that allows a certain amount of randomness in the wireless transmission latency without undermining the reliability of the communication system. It should be noted that the transmission latency, $T_{Latency}$, for a MaxStream 9XCite transceiver can be as low as 5ms. This lower latency makes the 9XCite transceiver more suitable for real-time feedback control applications compared with the 24XStream transceiver. However, the 9XCite transceiver may only be used in countries where the 900MHz band is for free public usage, such as the U.S., Canada, Mexico, South Korea, and Japan.

3. Centralized and Decentralized Time-delay Control Algorithms using Velocity Feedback

An optimal feedback control design normally requires adequate real-time structural response data to compute optimal control forces. For example, if a multi-story building is modeled by a lumped-mass structural system with actuators deployed among adjacent floors, real-time floor displacements and velocities that constitute the state-space vector are needed for a typical linear quadratic regulator (LQR) controller (Franklin *et al.*, 2003). However, due to instrumentation complexity and cost, not all structural response data may be available in practice. To address this difficulty, output feedback control methods can be used to provide an optimal control strategy under the constraint that only part of the state-space variables are measured in real-time. This section first presents the basic formulation of an optimal centralized output feedback control

solution and then proposes a modified algorithm that allows the output feedback gain matrix to be constrained. The output feedback gain matrix is then formulated for various decentralized control architectures using the constrained gain matrix algorithm detailed herein.

3.1 Formulation for Centralized Linear Output Feedback Control

The output feedback digital-domain LQR control solution can be briefly summarized as follows. For a lumped-mass structural model with *n* degrees-of-freedom (DOF) and *m* actuators, the system state-space equation considering *l* time steps of delay can be stated as:

$$\mathbf{z_d}[k+1] = \mathbf{A_d}\mathbf{z_d}[k] + \mathbf{B_d}\mathbf{p_d}[k-l], \text{ where } \mathbf{z_d}[k] = \begin{Bmatrix} \mathbf{x_d}[k] \\ \dot{\mathbf{x}}_\mathbf{d}[k] \end{Bmatrix} \tag{3}$$

Here, $\mathbf{z_d}[k]$ represents the $2n \times 1$ discrete-time state-space vector, $\mathbf{x_d}[k]$ is the relative (to the base) displacement of the structural degrees-of-freedom, $\mathbf{p_d}[k-l]$ is the delayed $m \times 1$ control force vector, $\mathbf{A_d}$ is the $2n \times 2n$ system matrix (containing the information about structural mass, stiffness and damping), and $\mathbf{B_d}$ is the $2n \times m$ actuator location matrix. The primary objective of the time-delay LQR problem is to minimize a global cost function, *J*, by selecting an optimal control force trajectory $\mathbf{p_d}$:

$$J\Big|_{\mathbf{p_d}} = \sum_{k=l}^{\infty} \left(\mathbf{z_d}^T[k]\mathbf{Q}\mathbf{z_d}[k] + \mathbf{p_d}^T[k-l]\mathbf{R}\mathbf{p_d}[k-l] \right), \text{ where } \mathbf{Q}_{2n\times 2n} \geq 0 \text{ and } \mathbf{R}_{m\times m} > 0 \tag{4}$$

In an output feedback control design, when control decisions are computed, only data in the system output vector $\mathbf{y_d}[k]$ are available. The output vector is defined by a $q \times 2n$ linear transformation, $\mathbf{D_d}$, to the state-space vector $\mathbf{z_d}[k]$:

$$\mathbf{y}_{\mathbf{d}}[k] = \mathbf{D}_{\mathbf{d}}\mathbf{z}_{\mathbf{d}}[k] \tag{5}$$

For example, if the relative velocities on all floors are measurable but no relative displacement is measurable, $\mathbf{D}_{\mathbf{d}}$ can be defined as:

$$\mathbf{D}_{\mathbf{d\_cen}} = [\mathbf{0}_{n\times n} \quad \vdots \quad \mathbf{I}_{n\times n}] \tag{6}$$

In another example, if only inter-story velocities between adjacent floors are measurable, the following output matrix $\mathbf{D}_{\mathbf{d}}$ can be used:

$$\mathbf{D}_{\mathbf{d\_dec}} = \begin{bmatrix} 0 & 0 & 0 & \vdots & 1 & 0 & 0 \\ 0 & 0 & 0 & \vdots & -1 & 1 & 0 \\ 0 & 0 & 0 & \vdots & 0 & -1 & 1 \end{bmatrix} \tag{7}$$

The $m \times q$ optimal gain matrix $\mathbf{G}_{\mathbf{d}}$ is required to provide a linear output feedback control:

$$\mathbf{p}_{\mathbf{d}}[k] = \mathbf{G}_{\mathbf{d}}\mathbf{y}_{\mathbf{d}}[k] \tag{8}$$

Chung *et al*. (1995) proposes a solution to the output feedback control problem with time delay (say, l time steps) by introducing a modified first-order difference equation:

$$\bar{\mathbf{z}}_{\mathbf{d}}[k+1] = \bar{\mathbf{A}}_{\mathbf{d}}\bar{\mathbf{z}}_{\mathbf{d}}[k] + \bar{\mathbf{B}}_{\mathbf{d}}\bar{\mathbf{p}}_{\mathbf{d}}[k] \tag{9}$$

in which the augmented state $\bar{\mathbf{z}}_{\mathbf{d}}[k]$ is assembled from the past l states as:

$$\bar{\mathbf{z}}_{\mathbf{d}}[k] = \begin{bmatrix} \mathbf{z}_{\mathbf{d}}[k] \\ \mathbf{z}_{\mathbf{d}}[k-1] \\ \vdots \\ \mathbf{z}_{\mathbf{d}}[k-l] \end{bmatrix}_{2n(l+1)\times 1} \tag{10}$$

This system is equivalent to the original system (Eq. 3) by proper definitions of the augmented matrices and vectors: $\bar{\mathbf{A}}_{\mathbf{d}}$ and $\bar{\mathbf{B}}_{\mathbf{d}}$ are the augmented state-space system matrices, $\bar{\mathbf{D}}_{\mathbf{d}}$ is the augmented output matrix, $\bar{\mathbf{Q}}$ is the augmented weighting matrix, and $\bar{\mathbf{Z}}_{\mathbf{d}l}$ is the second statistical moment of the augmented initial disturbance. As a result, the following nonlinearly coupled matrix equations are simultaneously solved for an optimal output feedback gain matrix $\mathbf{G}_{\mathbf{d}}$, the Lagrangian matrix, **L**, and a constant matrix, **H**:

$$\left(\bar{\mathbf{A}}_{\mathbf{d}} + \bar{\mathbf{B}}_{\mathbf{d}}\mathbf{G}_{\mathbf{d}}\bar{\mathbf{D}}_{\mathbf{d}}\right)^T \mathbf{H}\left(\bar{\mathbf{A}}_{\mathbf{d}} + \bar{\mathbf{B}}_{\mathbf{d}}\mathbf{G}_{\mathbf{d}}\bar{\mathbf{D}}_{\mathbf{d}}\right) - \mathbf{H} + \left(\bar{\mathbf{Q}} + \bar{\mathbf{D}}_{\mathbf{d}}{}^T\mathbf{G}_{\mathbf{d}}{}^T\mathbf{R}\mathbf{G}_{\mathbf{d}}\bar{\mathbf{D}}_{\mathbf{d}}\right) = \mathbf{0} \tag{11a}$$

$$\left(\bar{\mathbf{A}}_{\mathbf{d}} + \bar{\mathbf{B}}_{\mathbf{d}}\mathbf{G}_{\mathbf{d}}\bar{\mathbf{D}}_{\mathbf{d}}\right)\mathbf{L}\left(\bar{\mathbf{A}}_{\mathbf{d}} + \bar{\mathbf{B}}_{\mathbf{d}}\mathbf{G}_{\mathbf{d}}\bar{\mathbf{D}}_{\mathbf{d}}\right)^T - \mathbf{L} + \bar{\mathbf{Z}}_{\mathbf{d}l} = \mathbf{0} \tag{11b}$$

$$2\bar{\mathbf{B}}_{\mathbf{d}}{}^T\mathbf{H}\left(\bar{\mathbf{A}}_{\mathbf{d}} + \bar{\mathbf{B}}_{\mathbf{d}}\mathbf{G}_{\mathbf{d}}\bar{\mathbf{D}}_{\mathbf{d}}\right)\mathbf{L}\bar{\mathbf{D}}_{\mathbf{d}}{}^T + 2\mathbf{R}\mathbf{G}_{\mathbf{d}}\bar{\mathbf{D}}_{\mathbf{d}}\mathbf{L}\bar{\mathbf{D}}_{\mathbf{d}}{}^T = \mathbf{0} \tag{11c}$$

Interested readers are referred to Chung *et al*. (1995), where the time-delay optimal control solution is derived in detail.

3.2 Heuristic Solution for Centralized and Decentralized Output Feedback Gain Matrices

An iterative algorithm to solve the continuous-time feedback control problem has been presented by Lunze (1990). The algorithm (Fig. 5) starts from an initial estimate for the gain matrix $\mathbf{G}_{\mathbf{d}}$. Within each iteration step *i*, the matrix $\mathbf{H}_i$ and $\mathbf{L}_i$ are solved respectively using the current estimate of the gain matrix $\mathbf{G}_{\mathbf{d}i}$. Based on the $\mathbf{H}_i$ and $\mathbf{L}_i$ matrices computed, a searching gradient

$\mathbf{\Delta}_i$ is calculated and the new gain matrix $\mathbf{G}_{\mathbf{d}i+1}$ is computed by traversing along a gradient from $\mathbf{G}_{\mathbf{d}i}$. An adaptive multiplier, *s*, is used to dynamically control the search step size. At each iteration step, two conditions are used to decide whether $\mathbf{G}_{\mathbf{d}i+1}$ is an acceptable estimate. The first condition is $trace(\mathbf{H}_{i+1}\bar{\mathbf{Z}}_{\mathbf{d}l}) < trace(\mathbf{H}_i\bar{\mathbf{Z}}_{\mathbf{d}l})$ which guarantees that $\mathbf{G}_{\mathbf{d}i+1}$ is a better solution than $\mathbf{G}_{\mathbf{d}i}$. The second condition is that the maximum magnitude of all the eigenvalues of the matrix $\left(\bar{\mathbf{A}}_{\mathbf{d}} + \bar{\mathbf{B}}_{\mathbf{d}}\mathbf{G}_{\mathbf{d}i+1}\bar{\mathbf{D}}_{\mathbf{d}}\right)$ is less than 1 which ensures the stability of the augmented system.

The iterative algorithm put forth by Lunze (1990) has an inherently powerful and attractive feature; the algorithm can be used to formulate an optimal control solution for a decentralized system simply by constraining the structure of $\mathbf{G}_{\mathbf{d}}$ to be consistent with the decentralized architecture. The following equation presents the structure of two decentralized output feedback gain matrices for a simple 3-story lumped-mass structure.

$$\mathbf{G}_{\mathbf{d\_dec1}} = \begin{bmatrix} * & 0 & 0 \\ 0 & * & 0 \\ 0 & 0 & * \end{bmatrix}, \text{ and } \mathbf{G}_{\mathbf{d\_dec2}} = \begin{bmatrix} * & * & 0 \\ 0 & * & * \\ 0 & * & * \end{bmatrix} \tag{12}$$

The pattern in $\mathbf{G}_{\mathbf{d\_dec1}}$ specifies that when computing control decisions, the actuator on each floor only needs the entry in the output vector $\mathbf{y}_{\mathbf{d}}$ that corresponds to that floor. The pattern in $\mathbf{G}_{\mathbf{d\_dec2}}$ specifies that information from neighboring floors be considered in calculating control actions. In order to find a decentralized gain matrix that satisfies desired architectural constraints, the algorithm described in Fig. 5 is modified by zeroing out the entries in the gradient matrix $\mathbf{\Delta}_i$ corresponding to zero terms in the decentralized output feedback gain matrix. The next estimate $\mathbf{G}_{\mathbf{d}i+1}$ is computed by traversing along this constrained gradient. Using the above decentralized

gain matrices and the output matrix $\mathbf{D}_{d\_dec}$ defined in Eq. (7), inter-story velocities between adjacent floors can be used for the calculation of control actions in a decentralized control system.

3.3 Simulation Results using Centralized and Decentralized Control Strategies

Numerical simulations have been conducted to assess the performance of decentralized and centralized control strategies considering time delays due to communication latencies. A numerical model for the 3-story half-scale laboratory structure illustrated in Fig. 1 is used for the simulation. For simplicity, ideal structural actuators which are capable of producing any desired force under the maximum limit of 20kN is deployed between each pair of adjacent floors using the V-braces shown. Three control architectures are employed: (1) decentralized, (2) partially decentralized, and (3) centralized. Different patterns of the gain matrices, $\mathbf{G}_d$, and the output matrices, $\mathbf{D}_d$, for these three control architectures are summarized in Table 2. As defined by these matrices, one centralized and two decentralized velocity feedback patterns are adopted. An LQR weighting matrix $\mathbf{Q}$ minimizing inter-story drifts over time and a diagonal weighting matrix $\mathbf{R}$ are used when designing the optimal gain matrices for all the simulations presented herein. Various combinations of centralization degrees (1: fully decentralized; 2: partially decentralized; 3: centralized) and sampling time steps ranging from 0.005s to 0.1s (at a resolution of 0.005s) are simulated.

To assess the performance of each control scheme, three ground motion records are used for the simulation: 1940 El Centro NS (Imperial Valley Irrigation District Station), 1999 Chi-Chi NS (TCU-076 Station), and 1995 Kobe NS (JMA Station) earthquake records. Performance indices proposed by Spencer *et al*. (1998) are adopted. In particular, two representative performance indices employed are:

$$PI_1 = \max_{\substack{\text{El Centro}\\ \text{Kobe}\\ \text{Chichi}}} \left\{ \frac{\max\limits_{t,i} d_i(t)}{\max\limits_{t,i} \hat{d}_i(t)} \right\}, \text{ and } PI_2 = \max_{\substack{\text{El Centro}\\ \text{Kobe}\\ \text{Chichi}}} \left\{ \frac{J_{LQR}}{\hat{J}_{LQR}} \right\} \tag{13}$$

where PI_1 and PI_2 are the performance indices corresponding to inter-story drifts and LQR cost indices, respectively. In Eq. (13), $d_i(t)$ represents the inter-story drift between floor *i* (*i* = 1, 2, 3) and its lower floor at time *t*, and $\max\limits_{t,i} d_i(t)$ is the maximum inter-story drift over the entire time history and among all three floors. The maximum inter-story drift is normalized by its counterpart $\max\limits_{t,i} \hat{d}_i(t)$, the maximum response of the uncontrolled structure. The largest normalized ratio among the simulations for the three different earthquake records is defined as the performance index PI_1. Similarly, the performance index PI_2 is defined for the LQR control index J_{LQR}, as given in Eq. (4). When computing the LQR index over time, a uniform time step of 0.005s is used to collect the structural response data points, regardless of the sampling time step of the control scheme; this allows one control strategy to be compared to another without concern for the different sampling time steps used in the control solution.

Values of the two control performance indices are plotted in Fig. 6 for different combinations of centralization degrees and sampling time steps. The plots shown in Fig. 6(a) and 6(b) illustrate that centralization degree and sampling step have significant impact on the performance of the control system. Generally speaking, control performance is better for higher degrees of centralization and shorter sampling times. To better review the simulation results, the performance indices for the three different control schemes are re-plotted as a function of sampling time in Fig. 6(c) and 6(d). As shown in Fig. 6(c), if a partially decentralized control system can achieve 0.04s sampling step and a centralized system can only achieve 0.08s due to additional communication latency, the partially decentralized system can result in lower

maximum inter-story drifts. Similar trends are observed in Fig. 6(d), although for a given sampling time step, the performance index PI_2 for the centralized case is always lower than the indices for the two decentralized cases.

4. Validation Experiments using a 3-story Structure Instrumented with MR Dampers

To study the potential use of the wireless sensing and control system for decentralized structural control, validation tests are conducted at the National Center for Research on Earthquake Engineering (NCREE) in Taipei, Taiwan. The same test structure has been used in a previous wireless control study in which one MR damper is installed for closed-loop control (Lynch et al. 2006c). Both a baseline wired control system and a wireless sensing and control system are employed to implement the real-time feedback control of a 3-story steel frame instrumented with three MR dampers.

4.1 Validation Test Setup

A three-story steel frame structure is designed and constructed by researchers affiliated with NCREE (Fig. 7a). The dimensions of the structure are provided in Fig. 1. The three-story structure is mounted on a 5m × 5m 6-DOF shake table. The shake table can generate ground excitations with frequencies spanning from 0.1Hz to 50Hz. For this study, only longitudinal excitations are used. Along this direction, the shake table can excite the structure with a maximum acceleration of 9.8m/s^2. The excitation has a maximum stroke and force of ±0.25m and 220kN, respectively. The test structure and shake table are heavily instrumented with accelerometers, velocity meters, and linear variable displacement transducers (LVDT) to measure their dynamic response. These sensors are interfaced to a high-precision wire-based data acquisition (DAQ) system permanently installed in the NCREE facility; the DAQ system is set to a sampling rate of 200 Hz. A separate set of wireless sensors are installed as part of the wireless control system.

For the wireless system, a total of four wireless sensors are installed following the deployment strategy shown in Fig. 1. Each wireless sensor is interfaced to a Tokyo Sokushin VSE15-D velocity meter to measure the absolute velocity response of each floor of the structure as well as at the base (i.e. table top velocity). The sensitivity of the velocity meter is 10V/(m/s) with a measurement limit of ±1 m/s. The three wireless sensors on the first three levels of the structure (C_0, C_1, and C_2) are also responsible for commanding the MR dampers. Besides the wireless control system, a traditional wire-based control system is installed in the structure for comparative analyses. Centralized and decentralized velocity feedback control schemes described earlier (Table 2) are used for both the wired and the wireless control systems. As shown in Table 3, different decentralization patterns and sampling steps are tested. For the test structure, the wire-based system can achieve a sampling rate of 200Hz, or a time step of 0.005s. Mostly decided by the communication latency of the 24XStream wireless transceivers, the wireless system can achieve a sampling rate of 12.5Hz (or a time step of 0.08s) for the centralized control scheme. This sampling rate is due to each wireless sensor waiting in turn to broadcast its data to the network (about 0.02s for each transmission). An advantage of the decentralized architecture is that fewer communication steps are needed, thereby reducing the time for wireless communication. As shown in Table 3, the wireless system can achieve a sampling rate of 16.67Hz for partially decentralized control and 50Hz for fully decentralized control.

4.2 Magnetorheological (MR) Damper Hysteresis Model

For this experimental study, three 20 kN MR dampers are installed with V-braces on each story of the steel structure (Fig. 7b). The damping coefficients of the MR dampers can be changed in real-time by the wireless control units (Fig. 7(c)) simply by issuing a command voltage between 0 to 1.2V. A separate power module is needed to provide 24V of power to each MR damper. In addition, this power module takes the command voltage as an input and converts this command

signal to a regulated current from 0 to 2A. The current is input to the internal electromagnetic coil of the MR damper to generate a magnetic field that sets the viscous damping properties of the MR fluid contained within the damper cylinder. Therefore, the axial force required to move the damper piston against the cylinder is adjustable through the command voltage. Calibration tests are first conducted on the MR dampers before mounting them to the structure so that modified Bouc-Wen damper models can be formulated for each damper (Lin *et al*., 2005).

The nonlinear force-velocity relationship for this modified Bouc-Wen model is defined as:

$$F(t) = C(V)\dot{x}(t) + z(t) \tag{14}$$

where $F(t)$ is the force provided by the MR damper, $C(V)$ is the damping coefficient adjustable through the damper command voltage V, $\dot{x}(t)$ is the relative velocity of the damper piston against the cylinder, and $z(t)$ is the hysteresis restoring force of the damper. The hysteresis restoring force, $z(t)$, evolves according to the following differential equation (Lin *et al*., 2005):

$$\dot{z}(t) = A\dot{x}(t) + \sum_{n=1}^{N} a_n \left[\beta \left| \dot{x}(t) \right| \left| z(t) \right|^{n-1} z(t) + \gamma \dot{x}(t) \left| z(t) \right|^{n} \right] \tag{15}$$

where A, β, γ, a_n, and N are parametric constants of the Bouc-Wen model. The higher the order N, the more accurate the model is in describing the complicated hysteresis behavior of the semi-active damper. In this study, it was found that an order of $N = 2$ provides fairly accurate modeling to the damper hysteresis forces. The hysteresis restoring force in discrete-time form at step k is then rewritten as:

$$z[k] = z[k-1] + \boldsymbol{\Phi}^T[k-1]\boldsymbol{\Theta}(V) \tag{16a}$$

$$\boldsymbol{\Theta}(V) = \{\theta_1(V) \quad \theta_2(V) \quad \theta_3(V) \quad \theta_4(V) \quad \theta_5(V)\}^T \tag{16b}$$

$$\boldsymbol{\Phi}[k] = \Delta t\left\{\dot{x}[k] \quad |\dot{x}[k]|z[k] \quad \dot{x}[k]|z[k]| \quad |\dot{x}[k]||z[k]|z[k] \quad \dot{x}[k]|z[k]|^2\right\}^T \tag{16c}$$

The five parameters in vector $\boldsymbol{\Theta}(V)$ are modeled as low-order polynomial functions of the damper voltage *V*. Similarly, the damping coefficient, *C*(*V*), is modeled as a linear function of the damper voltage *V*. For each MR damper, the constant coefficients in the polynomial functions $\boldsymbol{\Theta}(V)$ and *C*(*V*) are pre-determined and validated through a series of calibration experiments with the damper (Lin *et al.*, 2005). In these experiments, a displacement-controlled actuator is employed to command displacements to the damper piston while the damper cylinder is fixed to a reaction frame. A load cell is then used to measure the damper force, so that the force-displacement time histories of the damper can be recorded. In order to compute the constant coefficients in the modified Bouc-Wen model, sinusoidal and random displacement are first applied to the damper with the damper command voltage fixed at multiple levels. Then the model is validated through experiments when random displacement time histories are applied to the damper with the command voltage randomly varied.

In the real-time feedback control tests, hysteresis status updating for the MR dampers is an integral element in the calculation of damper actuation voltages. At each sampling time step, a wireless control unit first decides the desired control force for the MR damper using the control algorithms described in Section 3 (Eq. 8). Meanwhile, the unit calculates the damper hysteresis status according to the modified Bouc-Wen model (Eq. 16). According to the hysteresis status, the wireless control unit decides the appropriate command voltage needed to be applied to the MR damper to attain a damping force closest to the desired control force. Fig. 8 illustrates the comparison between the control force desired by the wireless control units and the actual force

(as measured by the load cells) achieved by the MR dampers on Floor-0 and Floor-1 during a centralized control test. The ground excitation in this test is the 1940 El Centro NS earthquake record scaled to a peak ground acceleration of $1 m/s^2$. The strong similarity between the desired and achieved control forces validates the damper hysteresis computation accomplished by the wireless control units, and the effectiveness of the modified Bouc-Wen MR damper model.

4.3 Experimental Results

To ensure that appropriate control decisions are computed by the wireless control units, one necessary condition is that the real-time velocity data used by the control units are reliable. Rarely experiencing data losses during the experiments, our prototype wireless sensor network proves to be robust (as reported by Lynch et al. (2006c), data losses less than 2% are experienced). Should data loss be encountered, the wireless control unit is currently designed to simply use a previous data sample. To illustrate the reliability of the velocity data collected and transmitted by the wireless units, Fig. 9(a) presents the Floor-1 time history data during the same centralized wireless control test as presented in Fig. 8. The data is collected separately by the cabled DAQ system and recorded by the three wireless control units. During the test, unit C_1 measures the data from the associated velocity meter directly, stores the data in its own memory bank, and transfers the data wirelessly to unit C_0 and C_2. After the test run is completed, data from all the three control units are sequentially streamed to the experiment command server, where the results are plotted as shown in Fig. 9(a). These plots illustrate strong agreements among data recorded by the three wireless control units and by the cabled system using a separate set of velocity meters and data acquisition system. This result shows that the velocity data is not only reliably measured by unit C_0, but also properly transmitted to the other wireless control units in real-time.

The time histories of the inter-story drifts from the same centralized wireless control test are plotted in Fig. 9(b), together with the drifts of a centralized wired control test and a dynamic test

when the structure is not instrumented with any control system (i.e. the MR dampers are not yet installed). The same ground excitations (e.g. the 1940 El Centro NS earthquake record scaled to a peak ground acceleration of $1m/s^2$) are used for all the three cases shown in Fig. 9(b). The results show that both the wireless and wired control systems achieve considerable gain in limiting inter-story drifts. Running at a much shorter sampling time step, the wired centralized control system achieves slightly better control performance than the wireless centralized system in terms of mitigating inter-story drifts.

To further study different decentralized schemes with different communication latencies, Fig. 10 shows the peak inter-story drifts and floor accelerations for the original uncontrolled structure and the structure controlled by the four different wireless and wired control schemes, as defined in Table 3. Three earthquake records, the 1940 El Centro NS, 1999 Chi-Chi NS, and 1995 Kobe NS records, are employed for the experimental tests, with their peak ground accelerations all scaled to $1m/s^2$. Compared with the uncontrolled structure, all wireless and wired control schemes achieve significant reduction with respect to maximum inter-story drifts and absolute accelerations. Among the four control cases, the wired centralized control scheme shows good performance in mitigating both peak drifts and peak accelerations. For example, when the 1940 El Centro NS earthquake is employed (Fig. 10a), the wired centralized control scheme achieves the smallest peak drifts and second smallest overall peak accelerations. This result is expected because the wired system has the advantages of lower communication latency and utilizes sensor data from all floors (complete state data). The wireless schemes, although running at longer sampling steps, achieve control performance comparable to the wired system. For all three earthquake records, the fully decentralized wireless control scheme (case #1) results in low peak inter-story drifts and the smallest peak floor accelerations at most of the floors. This result illustrates that in the decentralized wireless control cases, the higher sampling rate (achieved due

to lower communication latency) potentially compensates for the lack of data available since sensor data from faraway floors is ignored.

5. Summary and Conclusions

This paper investigates the feasibility and effectiveness of decentralized wireless control strategies in civil structures. The adoption of wireless telemetry for structural control applications is advantageous because it reduces the need for wiring between sensors, actuators and controllers yet it offers flexible communication architectures with modifiable network topologies. A prototype wireless structural sensing and control system designed for real-time civil structural control is first introduced. We then present the theoretical background for an optimal output feedback structural control design using centralized and decentralized communication patterns. Both numerical simulations and experimental tests are performed to examine the tradeoff between the "degree" of centralization and communication latencies. The simulated and experimental results show that decentralized wireless control strategies may provide equivalent or even superior control performance, given that their centralized counterparts suffer longer sampling steps due to wireless communication latencies. Laboratory experiments also successfully validate the reliability of the prototype wireless structural sensing and control system. With larger-scale control systems (defined by higher nodal densities) encountering greater communication complexities (i.e. communication delays, data loss, and limited communication range), more work is needed to explore the tradeoffs between degree of decentralization, sample rate and global control system performance.

Acknowledgments

This research is partially funded by the National Science Foundation under grants CMS-9988909 (Stanford University), CMS-0528867 (University of Michigan), and the Office of Naval Research Young Investigator Program awarded to Prof. Lynch at the University of Michigan. Additional

support is provided by National Science Council in Taiwan under Grant No. NSC 94-2625-Z-002-031. The authors wish to thank the two fellowship programs: the Office of Technology Licensing Stanford Graduate Fellowship and the Rackham Grant and Fellowship Program at the University of Michigan.

Reference

Celebi, M. (2002), *Seismic Instrumentation of Buildings (with Emphasis on Federal Buildings)*, Report No. 0-7460-68170, United States Geological Survey (USGS), Menlo Park, CA, USA.

Chu, S.Y., Soong, T.T. and Reinhorn, A.M. (2005), *Active, Hybrid and Semi-active Structural Control*, John Wiley & Sons Ltd, West Sussex, England.

Chung, L.L., Lin, C.C. and Lu, K.H. (1995), "Time-delay Control of Structures," *Earthquake Engineering & Structural Dynamics*, **24**(5), 687-701.

Eker, J., Cervin, A. and Hörjel, A. (2001), "Distributed Wireless Control Using Bluetooth," *Proc. of IFAC Conf. on New Technologies for Control System*, Hong-Kong, China, November 19-22, 2001.

Franklin, G.F., Powell, J.D. and Workman, M. (2003), *Digital Control of Dynamic Systems*, Pearson Education, New Jersey.

Lian, F.-L., Moyne, J. and Tilbury, D. (2002), "Network Design Consideration for Distributed Control Systems," *IEEE Transactions on Control Systems Technology*, **10**(2), 297-307.

Lin, P.-Y., Roschke, P.N. and Loh, C.-H. (2005). "System Identification and Real Application of a Smart Magneto-Rheological Damper," *Proc. of the 2005 International Symposium on Intelligent Control*, Limassol, Cyprus, June 27-29, 2005.

Lunze, J. (1992), *Feedback Control of Large-scale Systems*, Prentice Hall, Hertfordshire, UK.

Lynch, J.P. and Law, K.H. (2002). "Decentralized Control Techniques for Large-scale Civil Structural Systems," *Proc. of the 20th International Modal Analysis Conf.*, Los Angeles, CA, USA, February 4-7, 2002.

Lynch, J.P. and Tilbury, D. (2005), "Implementation of a Decentralized Control Algorithm Embedded within a Wireless Active Sensor," *Proc. of the 2nd Annual ANCRiSST Workshop*, Gyeongju, Korea, July 21-24, 2005.

Lynch, J.P. and Loh, K. (2006a), "A Summary Review of Wireless Sensors and Sensor Networks for Structural Health Monitoring," *Shock and Vibration Digest*, **38**(2), 91-128.

Lynch, J.P., Wang, Y., Loh, K., Yi, J., and Yun, C.-B. (2006b), "Performance Monitoring of the Geumdang Bridge using a Dense Network of High-Resolution Wireless Sensors," *Smart Materials and Structures*, IOP, **15**(6), 1561-1575..

Lynch, J.P., Wang, Y., Swartz, R. A., Lu, K. C., and Loh, C. H. (2006c). "Implementation of a Closed-Loop Structural Control System using Wireless Sensor Networks," *Journal of Structural Control and Health Monitoring*, Wiley, in review.

MaxStream, Inc. (2005). *XStream™ OEM RF Module Product Manual*, Lindon, UT, USA.

Ploplys, N.J., Kawka, P.A. and Alleyne, A.G. (2004), "Closed-loop Control over Wireless Networks," *IEEE Control Systems Magazine*, **24**(3), 58-71.

Sandell, N., Jr., Varaiya, P., Athans, M. and Safonov, M., "Survey of Decentralized Control Methods for Large Scale Systems", *IEEE Transactions on Automatic Control*, **23**(2), 108-128.

Seth, S., Lynch, J.P. and Tilbury, D., "Feasibility of Real-Time Distributed Structural Control upon a Wireless Sensor Network," *Proceedings of the 42nd Annual Allerton Conference on Communication, Control and Computing*, Allerton, IL, USA, September 29 - October 1, 2004.

Solomon, I., Cunnane, J. and Stevenson, P. (2000). "Large-scale Structural Monitoring Systems," *Proc. of SPIE Non-destructive Evaluation of Highways, Utilities, and Pipelines IV*, Newport Beach, CA, March 7-9, 2000.

Soong, T.T. and Spencer, B.F., Jr. (2002). "Supplemental Energy Dissipation: State-of-the-art and State-of-the-practice," *Engineering Structures*, **24**(3), 243-259.

Spencer, B.F., Jr., Christenson, R.E. and Dyke, S.J., (1998). "Next Generation Benchmark Control Problem for Seismically Excited Buildings." *Proc. of 2nd World Conf. on Structural Control*, Kyoto, Japan, June 29 -July 2, 1998.

Straser, E.G. and Kiremidjian, A.S. (1998), *A Modular, Wireless Damage Monitoring System for Structures*, Report No. 128, John A. Blume Earthquake Eng. Ctr., Stanford University, Stanford, CA, USA.

Wang, Y., Swartz, A., Lynch, J.P., Law, K.H., Lu, K.-C. and Loh, C.-H. (2006), "Wireless Feedback Structural Control with Embedded Computing," *Proc. of the SPIE 11th International Symposium on Nondestructive Evaluation for Health Monitoring and Diagnostics*, San Diego, CA, USA, February 26 - March 2, 2006.

Wang, Y., Lynch, J.P. and Law, K.H. (2007), "A Wireless Structural Health Monitoring System with Multithreaded Sensing Devices: Design and Validation," *Structure and Infrastructure Engineering - Maintenance, Management and Life-Cycle Design & Performance*, **3**(2), 103-120.

Key words: structural control, wireless communication, embedded computing, decentralized control, velocity feedback control

List of Figures and Tables

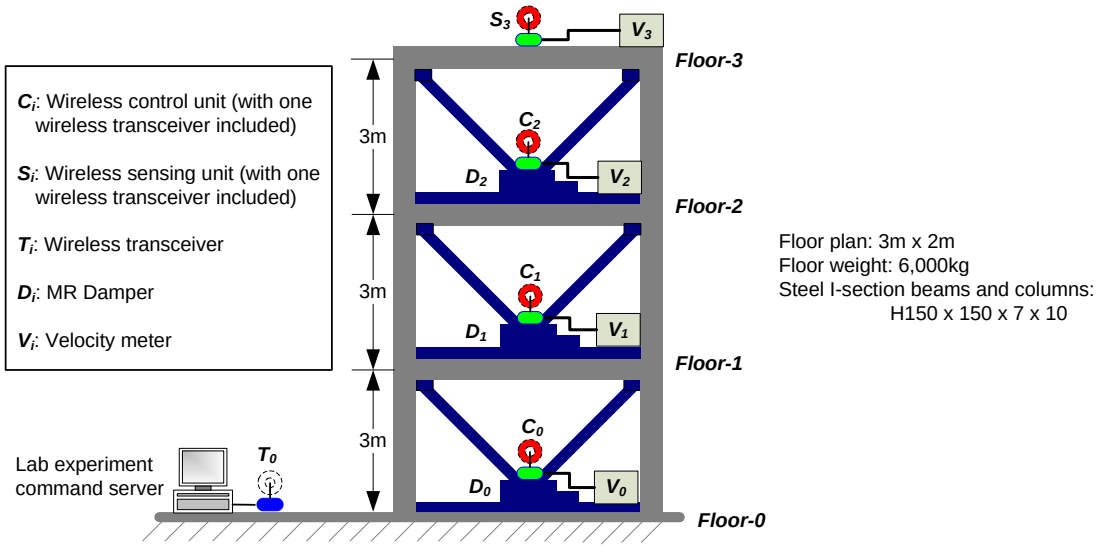

Figure 1. Illustration of the prototype wireless sensing and control system using a 3-story structure controlled by three MR dampers.

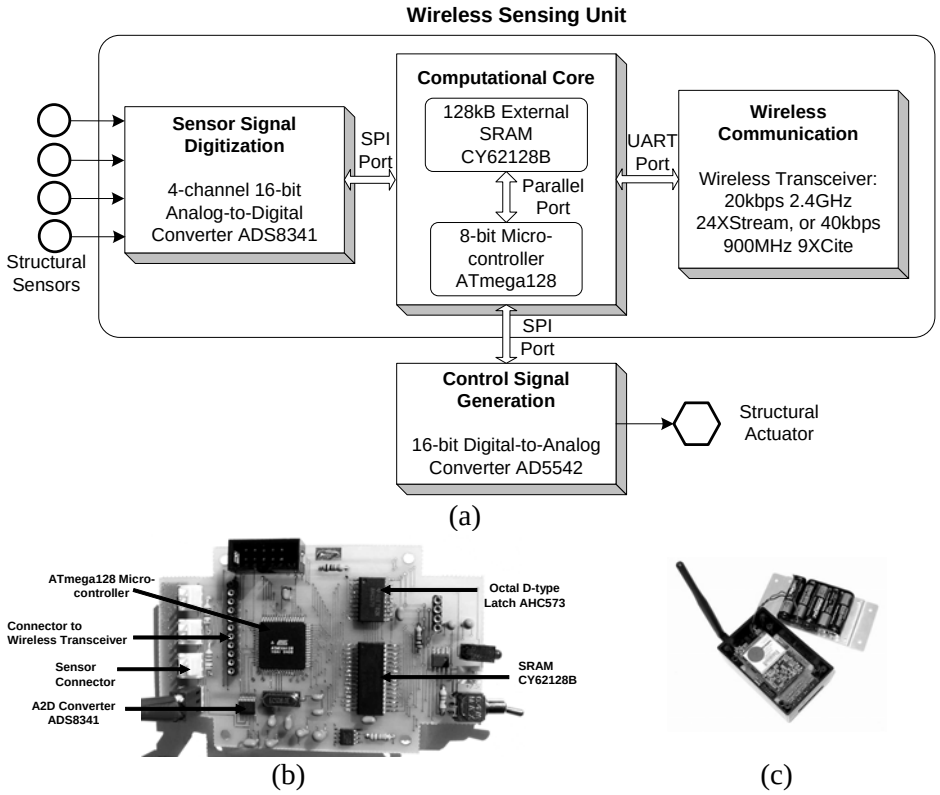

Figure 2. Wireless sensing unit: (a) functional diagram detailing the hardware design of the wireless sensing unit interfaced with the actuation signal generation module; (b) printed circuit board for the wireless sensing unit (9.7×5.8 cm^2); (c) package of the wireless sensing unit ($10.2 \times 6.5 \times 4.0$ cm^3).

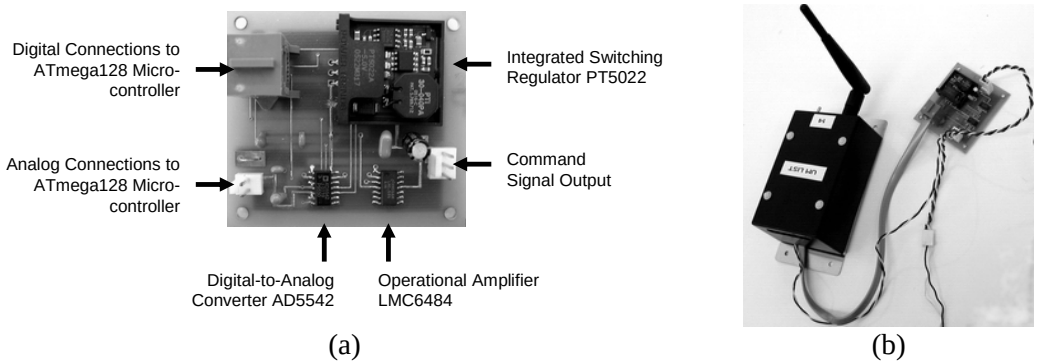

Figure 3. Pictures of the control signal module: (a) PCB board (5.5 × 6.0 cm^2); (b) control signal module connected to wireless sensor.

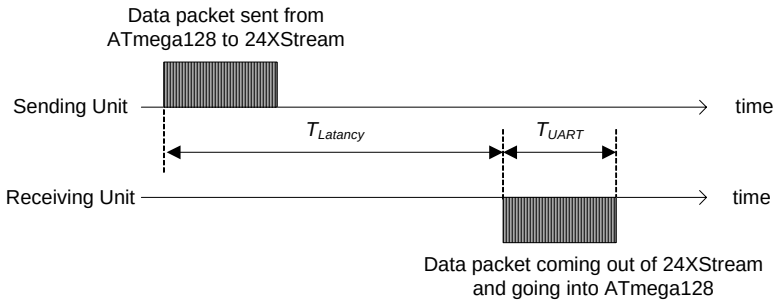

Figure 4. Communication latency of a single wireless transmission.

$\mathbf{G}_{\mathbf{d}1} = [\mathbf{0}]_{m\times q}$;
s = 1;
for i = 1,2,…
    Solve equation (11a) for $\mathbf{H}_i$;
    Solve equation (11b) for $\mathbf{L}_i$;
    Find gradient using equation (11c): $\boldsymbol{\Delta}_i = -\left(2\bar{\mathbf{B}}_{\mathbf{d}}{}^T\mathbf{H}\left(\bar{\mathbf{A}}_{\mathbf{d}} + \bar{\mathbf{B}}_{\mathbf{d}}\mathbf{G}_{\mathbf{d}}\bar{\mathbf{D}}_{\mathbf{d}}\right)\mathbf{L}\bar{\mathbf{D}}_{\mathbf{d}}{}^T + 2\mathbf{R}\mathbf{G}_{\mathbf{d}}\bar{\mathbf{D}}_{\mathbf{d}}\mathbf{L}\bar{\mathbf{D}}_{\mathbf{d}}{}^T\right)$;
    iterate {
        $\mathbf{G}_{\mathbf{d}i+1} = \mathbf{G}_{\mathbf{d}i} + s\cdot\boldsymbol{\Delta}_i$;
        Solve equation (11a) again for $\mathbf{H}_{i+1}$ using $\mathbf{G}_{\mathbf{d}i+1}$;
        if $trace(\mathbf{H}_{i+1}\bar{\mathbf{Z}}_{\mathbf{d}l})$ < $trace(\mathbf{H}_i\bar{\mathbf{Z}}_{\mathbf{d}l})$ and $\max\left(\left|eigen\left(\bar{\mathbf{A}}_{\mathbf{d}} + \bar{\mathbf{B}}_{\mathbf{d}}\mathbf{G}_{\mathbf{d}i+1}\bar{\mathbf{D}}_{\mathbf{d}}\right)\right|\right)$ < 1
            exit the **iterate** loop;
        else
            s = s / 2;
            If (s < machine precision), then **exit** the **iterate** loop;
        end
    };
    s = s × 2;
    If $\left\|\mathbf{G}_{\mathbf{d}i+1} - \mathbf{G}_{\mathbf{d}i}\right\|$ < acceptable error, then **exit** the **for** loop;
end

Figure. 5. Heuristic algorithm solving the coupled nonlinear matrix equations (Eq. 11) for centralized optimal time-delay output feedback control (Lunze, 1990).

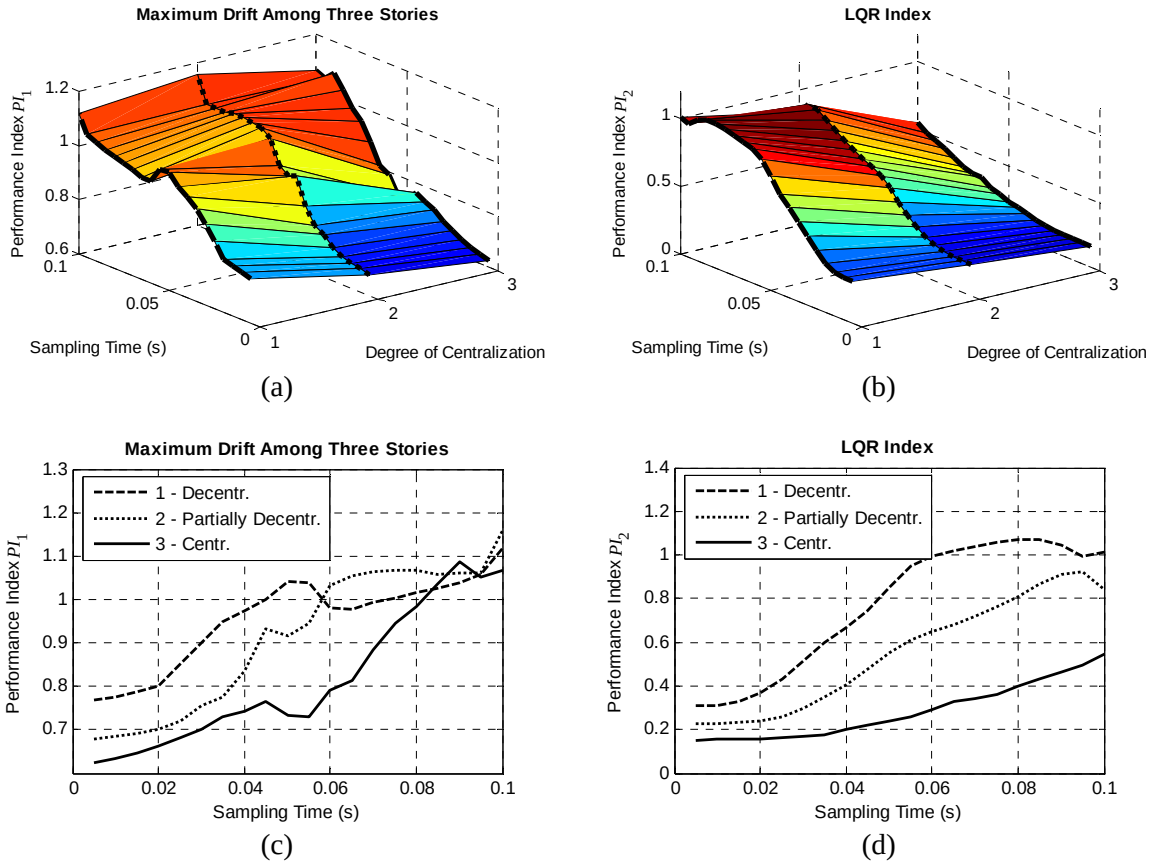

Figure 6. Simulation results illustrating control performance indexes for different sampling time steps and centralization degrees: (a) 3D plot for performance index PI_1; (b) 3D plot for performance index PI_2; (c) condensed 2D plot for PI_1; (d) condensed 2D plot for PI_2.

(a)

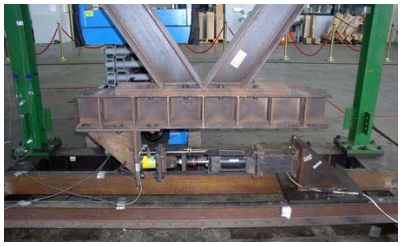

(b)

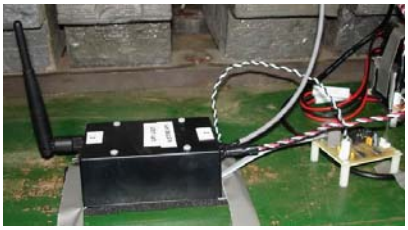

(c)

Figure 7. Laboratory setup: (a) the 3-story test structure mounted on the shake table; (b) the MR damper installed between the 1st floor and the base floor of the structure; (c) a wireless control unit and an off-board control signal generation module.

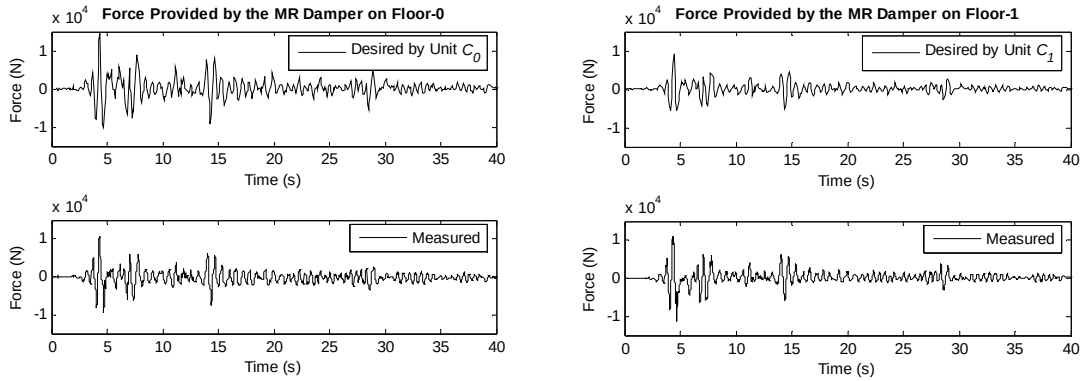

(a) (b)

Figure 8. Damper forces desired by the control units and achieved by the MR dampers during an experiment run: (a) force provided by the MR damper on Floor-0; (b) force provided by the MR damper on Floor-1.

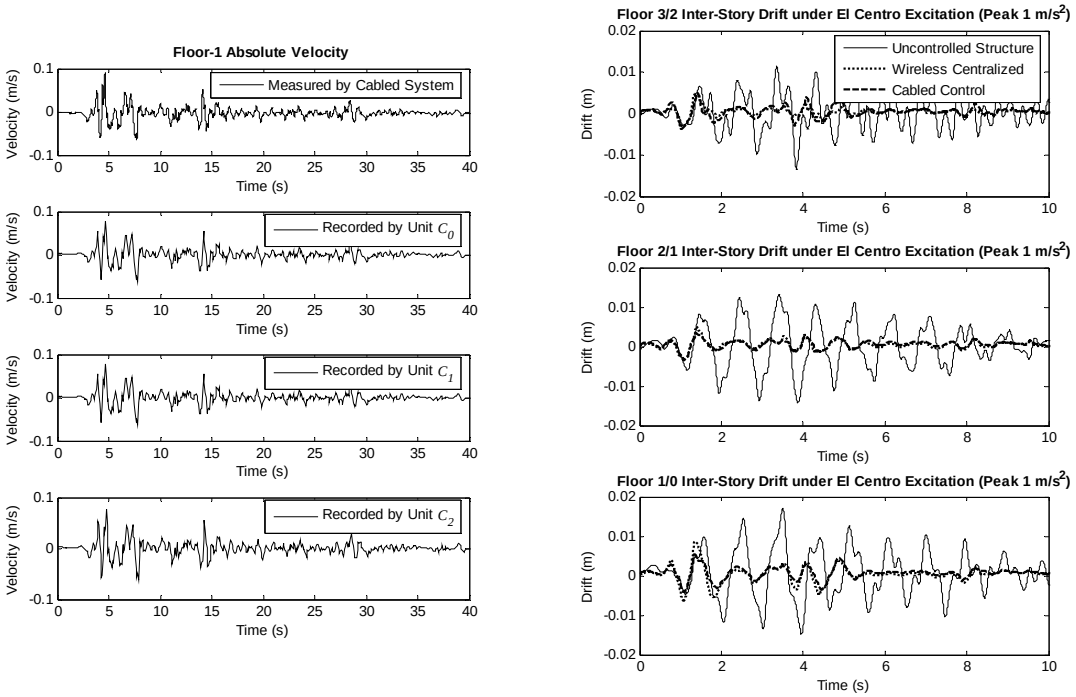

(a) (b)

Figure 9. Experimental time histories for: (a) Floor-1 absolute velocity data recorded by the cabled and wireless sensing systems; (b) inter-story drifts of the structure with and without control.

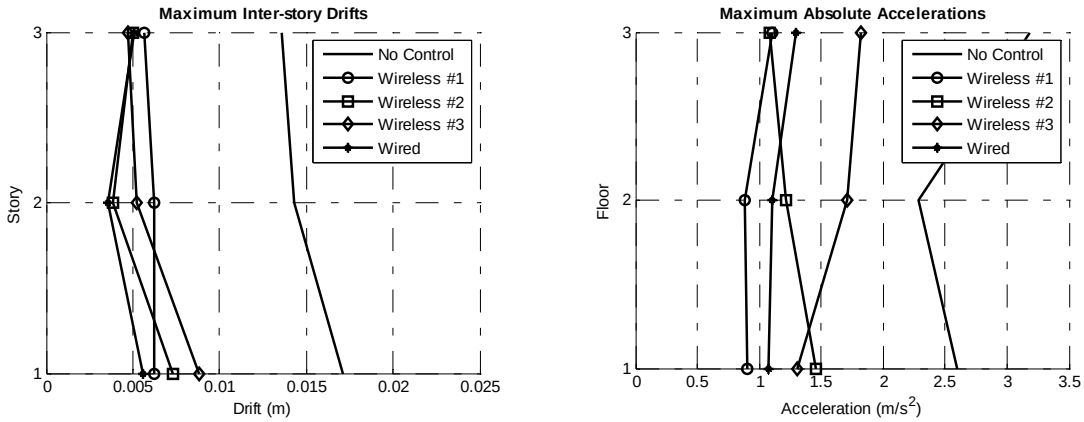

(a)

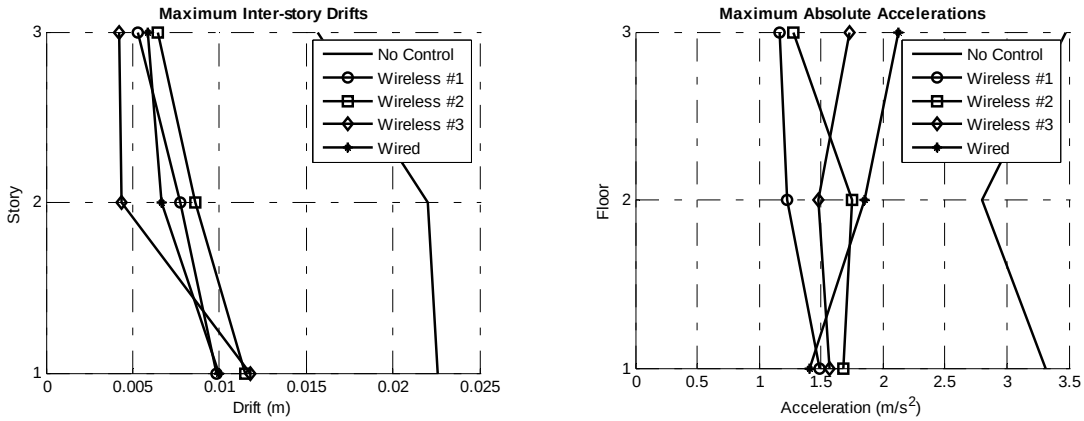

(b)

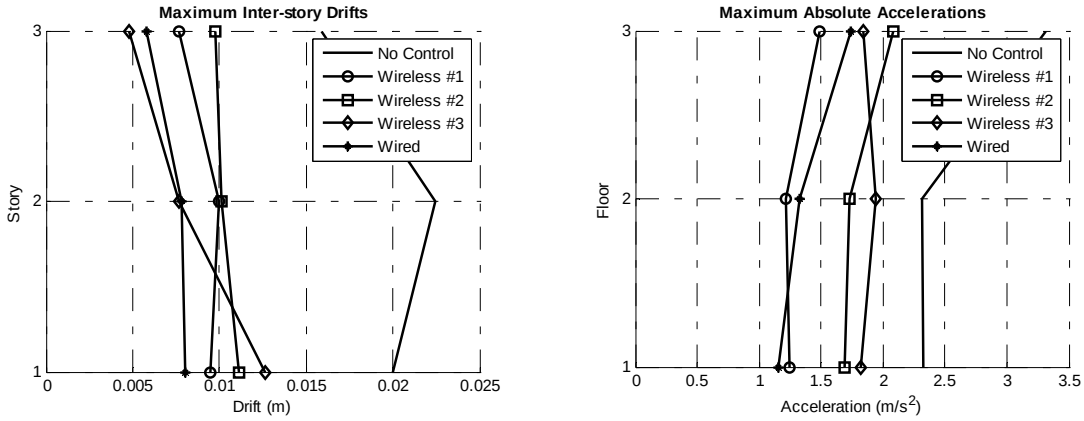

(c)

Figure 10. Experimental results of different control schemes under three earthquake excitations scaled to peak ground accelerations of 1m/s^2: (a) 1940 El Centro NS; (b) 1999 Chi-Chi NS; (c) 1995 Kobe NS.

Table 1. Key performance parameters of the wireless transceivers.

Specification	9XCite	24XStream
Operating Frequency	ISM 902-928 MHz	ISM 2.4000 – 2.4835 GHz
Channel Mode	7 frequency hopping channels, or 25 single frequency channels	7 frequency hopping channels
Data Transfer Rate	38.4 kbps	19.2 kbps
Communication Range	Up to 300' (90m) indoor, 1000' (300m) at line-of-sight	Up to 600' (180m) indoor, 3 miles (5km) at line-of-sight
Supply Voltage	2.85VDC to 5.50VDC	5VDC (±0.25V)
Power Consumption	55mA transmitting, 35mA receiving, 20μA standby	150mA transmitting, 80mA receiving, 26μA standby
Module Size	1.6" × 2.825" × 0.35" (4.06 × 7.17 × 0.89 cm^3)	1.6" × 2.825" × 0.35" (4.06 × 7.17 × 0.89 cm^3)
Network Topology	Peer-to-peer, broadcasting	Peer-to-peer, broadcasting

* For details about the transceivers, see http://www.maxstream.net.

Table 2. Different decentralization patterns for the control simulations and experiments.

Degree of Centralization	(1) Decentralized	(2) Partially Decentralized	(3) Centralized
Gain Matrix Constraint	$\mathbf{G}_{\mathbf{d\_dec1}}$ in Eq. (12)	$\mathbf{G}_{\mathbf{d\_dec2}}$ in Eq. (12)	N/A
Output Matrix	$\mathbf{D}_{\mathbf{d\_dec}}$ in Eq. (7)	$\mathbf{D}_{\mathbf{d\_dec}}$ in Eq. (7)	$\mathbf{D}_{\mathbf{d\_cen}}$ in Eq. (6)

Table 3. Different decentralization patterns and sampling steps for the wireless and wire-based control experiments (degrees of centralization are defined as shown in Table 2).

	Wireless System			Wired System
Degree of Centralization	1	2	3	3
Sampling Step/Rate	0.02s / 50Hz	0.06s / 16.67Hz	0.08s / 12.5Hz	0.005s / 200Hz